THE JOURNAL OF BIOLOGICAL CHEMISTRY VOL. 285, NO. 25, pp. 19660–19667, June 18, 2010

Laser-induced Propagation and Destruction of Amyloid β Fibrils*[S]

Received for publication, October 16, 2009, and in revised form, April 18, 2010 Published, JBC Papers in Press, April 20, 2010, DOI 10.1074/jbc.M109.076505

Hisashi Yagi[‡], Daisaku Ozawa[‡], Kazumasa Sakurai[‡], Toru Kawakami[‡], Hiroki Kuyama[‡], Osamu Nishimura[‡], Toshinori Shimanouchi[§], Ryoichi Kuboi[§], Hironobu Naiki[¶], and Yuji Goto[‡1]

From the [‡]Institute for Protein Research, Osaka University, Yamadaoka 3-2, Suita, Osaka 565-0871, Japan, the [§]Department of Engineering Science, Graduate School of Chemical Science and Engineering, Osaka University, 1-3, Machikaneyama-cho, Toyonaka, Osaka 560-8531, Japan, and the [¶]Department of Pathological Sciences, Faculty of Medical Sciences, University of Fukui, Matsuoka, Fukui 910-1193, Japan

The amyloid deposition of amyloid β (Aβ) peptides is a critical pathological event in Alzheimer disease (AD). Preventing the formation of amyloid deposits and removing preformed fibrils in tissues are important therapeutic strategies against AD. Previously, we reported the destruction of amyloid fibrils of β_2-microglobulin K3 fragments by laser irradiation coupled with the binding of amyloid-specific thioflavin T. Here, we studied the effects of a laser beam on Aβ fibrils. As was the case for K3 fibrils, extensive irradiation destroyed the preformed Aβ fibrils. However, irradiation during spontaneous fibril formation resulted in only the partial destruction of growing fibrils and a subsequent explosive propagation of fibrils. The explosive propagation was caused by an increase in the number of active ends due to breakage. The results not only reveal a case of fragmentation-induced propagation of fibrils but also provide insights into therapeutic strategies for AD.

The deposition of amyloid fibrils in extra- and intracellular spaces is associated with various amyloidoses, including Alzheimer disease (AD),[2] Parkinson, and Huntington diseases and dialysis-related amyloidosis (1–3). Moreover, several cases suggest that amyloid fibrils also have a normal biological function, contributing to normal cell and tissue physiology as functional amyloids (3–5). Thus, clarifying amyloidogenesis has an increasing importance for comprehensive understanding of normal and abnormal functions of proteins in life. Amyloidogenic proteins and peptides have been assumed to form amyloid fibrils via a common mechanism of nucleation and extension (6), creating various supramolecular assemblies (7–9). Recently, fragmentation has been proposed to play an important role in the propagation of fibrils (10–13). Additionally, a secondary mechanism of nucleation whereby new fibrils grow from existing ones has been suggested (11, 14). In the case of yeast Sup35 protein, the chaperon Hsp40/70 system disaggregates fibrillar Sup35 into oligomeric species for transmission from mother to daughter cells (15, 16). Such evidence suggests that the propagation of fibrils is a more dynamic process than that assumed on the basis of a simple process of nucleation and growth (13). To clarify the mechanism of propagation, direct observation is needed.

To directly observe the growth of fibrils, we developed a unique method combining total internal reflection fluorescence microscopy (TIRFM) with thioflavin T (ThT), an amyloid-specific fluorescence dye (6, 8, 9, 17, 18). This approach can provide information about the formation of individual fibrils in real time. Previously, we showed that a laser beam used for monitoring amyloid fibrils in the presence of ThT inhibited the growth of β_2-microglobulin fibrils and moreover caused the destruction of preformed fibrils of the 22-residue K3 fragment of β_2-microglobulin (19). We suggested that active oxygen generated by the excitation of ThT played a critical role in the destruction of the fibrils along with various chemical modifications. Because ThT binds to amyloid fibrils in common, this approach might help prevent various types of amyloidoses, although it is also reported the oxidation of amyloidogenic proteins or peptides accelerates fibril formation (20–22).

In this study, we examined the possibility that the lasers are useful for destroying Aβ amyloid fibrils. We first visualized the spontaneous fibril formation of Aβ(1–40), in which cleavage of fibrils during the initial stages caused subsequent explosive growth. On the other hand, the preformed fibrils were broken down by extensive irradiation, indicating that a laser is useful against preformed Aβ fibrils. We suggest that the effects of the irradiation are determined by a balance between the laser-induced acceleration of propagation and destruction, leading to a dependence with an optimum of propagation against the energy of the laser. Considering that self-propagation is intrinsic to amyloid fibrils, a dependence with an optimum may be common to various structural perturbants of amyloid fibrils giving important insights into therapeutic strategies for preventing amyloidosis.

EXPERIMENTAL PROCEDURES

Direct Observation of Amyloid Fibrils—The TIRFM system used to observe individual amyloid fibrils was developed based on an inverted microscope (IX70, Olympus, Tokyo, Japan) as

* This work was supported by grants-in-aid from the Japanese Ministry of Education, Culture, Sports, Science and Technology on priority areas and by the Japan Society for the Promotion of Science Research fellowships for young scientists (to H. Y.).

[S] The on-line version of this article (available at http://www.jbc.org) contains supplemental Figs. S1–S8 and Movies S1–S5.

[1] To whom correspondence should be addressed: Yamadaoka 3-2, Suita, Osaka 565-0871, Japan. Tel.: 81-6-6879-8614; Fax: 81-6-6879-8616; E-mail: ygoto@protein.osaka-u.ac.jp.

[2] The abbreviations used are: AD, Alzheimer disease; Aβ, amyloid β; TIRFM, total internal reflection fluorescence microscopy; ThT, thioflavin T; MALDI, matrix-assisted laser desorption ionization.

described (17, 18, 23). The ThT molecule was excited at 442 nm by a helium-cadmium laser (IK5552R-F, Kimmon, Tokyo, Japan). The fluorescence image was filtered with a band pass filter (D490/30, Omega Optical, Brattleboro, VT) and visualized using a digital steel camera (DP70, Olympus). The peptides were dissolved in an ammonia solution (0.05% for Aβ(1–40)) to 500 μM. Aβ(1–40) (50 μM) was incubated in a 50 mM sodium phosphate buffer, pH 7.5 containing 0.5 M NaCl and 0.5 mM SDS. Then, 100 μM ThT was added at a final concentration of 5 μM. An aliquot (14 μl) of sample solution was immediately deposited on a microscopic slide and incubated at 37 °C for 1–2 days, and an image of the fibrils was obtained with TIRFM.

Effects of Laser Irradiation on Preformed Aβ(1–40) Fibrils—To examine the effect of the laser, intermittent irradiation of Aβ(1–40) fibrils was performed. The fibrils formed on the quartz surface were irradiated by a helium-cadmium laser of 60 milliwatt for a 3–5 s duration. For the experiment of extensive laser irradiation on preformed fibrils, Aβ(1–40) fibrils were prepared on quartz slides in the absence of irradiation. The elongated fibrils were then irradiated at an intensity of 10–55 milliwatt for 1 min. It should be noted that the irradiation points were also the observation points. Fluorescence images of amyloid fibrils were obtained by TIRFM.

To clarify the effect of the laser beam on Aβ(1–40) fibrils in detail, light scattering and ThT assay (24) measurements were performed in bulk. To make Aβ(1–40) fibrils, Aβ(1–40) (50 μM) was incubated in 50 mM phosphate buffer (pH 7.5) containing 0.1 M NaCl or 0.5 M NaCl and 0.5 mM SDS in a test tube at 37 °C. The preformed Aβ(1–40) fibrils were diluted 20-fold with each polymerization buffer, and then a 100 μM ThT solution was added (final concentration, 5 μM). The samples were introduced into a glass cell with a 10-mm light path and then set on the TIRFM stage at 37 °C. The samples were irradiated by a helium-cadmium laser at 442 nm (30–40 milliwatt) with continuous agitation. The irradiated Aβ(1–40) fibrils were examined by monitoring light scattering (both set at 350 nm) and ThT fluorescence (excitation 445 nm and emission 490 nm) intensities. These measurements were made with a Hitachi F-7000 spectrofluorometer (Tokyo, Japan) at 37 °C.

Quantification of Fibril Images Visualized with TIRFM—We quantified the fluorescence images of amyloid fibrils visualized with TIRFM to obtain the time courses of fibril propagation or destruction. TIRFM pictures are made of pixels with respective fluorescence intensities. For each TIRFM picture, we took a histogram of the fluorescence intensity and fitted the histogram by multi-Gaussian. Then, from the Gaussian peak with the lowest peak intensity, we obtained the average signal intensity of background ($\langle I_{bkg} \rangle$) and its S.D. (σ_{bkg}). We counted the number of pixels whose intensity was larger than the threshold value of $\langle I_{bkg} \rangle + 5\sigma_{bkg}$ as the quantity of the fibril formed. Obtained values were normalized with respect to the initial intensity within each observation period.

Ultracentrifugation Measurements—The Aβ(1–40) fibrils with or without laser irradiation for 40 h were measured using a Beckman-Coulter Optima XL-1 analytical ultracentrifugation (Fullerton, CA) with an An-60 rotor and two-channel charcoal-filled Epon cells. The experiments were performed at 4 °C. After precentrifugation at 3,000 (664 × *g*) rpm, the rotor speed was increased to 45,000–53,000 rpm (149,420–207,270 × *g*), and absorbance data at 280 nm were collected at intervals of 2 (3000 rpm), 8 (45,000 rpm), and 30 min (53,000 rpm).

Amino Acid Analysis—The amino acid analysis was performed on a Hitachi L-2000 amino acid analyzer after hydrolysis with constant boiling point HCl at 110 °C for 24 h and 48 h in an evacuated sealed tube. High pressure liquid chromatography was carried out on a cation ion exchange column. The amino acids were detected by the reaction with ninhydrin.

Mass Spectrometry Analysis—MALDI mass spectra were recorded on AXIMA CFR-plus (SHIMADZU/KRATOS, Manchester, UK) reflection time-of-flight mass spectrometers equipped with a nitrogen laser (337 nm, 3 ns pulse width). All measurements were performed in a positive ion reflection mode. The ion acceleration voltage was set to 20 kV, and the reflection detector was operated at 24 kV. The flight path in the reflection mode is ~240 cm for both instruments.

For mass analysis, all of the Aβ(1–40) fibril samples were acidified with 0.1% trifluoroacetic acid solution and desalted using ZipTip (C-18). The fibrils were eluted with 50% (v/v) acetonitrile containing 0.05% (v/v) trifluoroacetic acid. α-Cyano-4-hydroxycinnamic acid was used as a matrix, which was dissolved to saturation in 50% (v/v) acetonitrile containing 0.05% (v/v) trifluoroacetic acid. An aliquot (0.5 μl) of sample solution was mixed with an equivalent volume of matrix solution on the MALDI target plate and analyzed after drying. The *m*/*z* values in the spectra were externally calibrated with angiotensin II (human) and insulin (bovine) using α-cyano-4-hydroxycinnamic acid as a matrix.

RESULTS

Propagation of Aβ(1–40) Fibrils—We carried out real-time observations by TIRFM of the spontaneous fibril formation of Aβ(1–40) at 50 μM and pH 7.5 at 37 °C in the presence of 5 μM ThT (Fig. 1). It is noted that 0.5 mM SDS was added to accelerate the fibril formation (8). In comparison with the seed-dependent growth of Aβ(1–40) (17), the spontaneous growth from monomers occurred much less frequently, requiring >8 h for the first fibrils to appear. In one case, a single fibril as long as 30 μm with a hairpin-like morphology was detected at 11 h (Fig. 1*A*, 11 h). Clear images of a long fibril against a dark background indicated that nucleation is rare under the conditions and that, once a nucleus forms, the fibril grows without the concomitant growth of neighboring fibrils. We did not observe oligomers or related globular precursors, suggesting that such precursors, even if accumulated, do not interact with ThT strongly enough to be detected by our method. Anticipating further growth, we focused on this single fibril. Surprisingly, the fibril self-cleaved into many fragments after 1 h (Fig. 1*A*, 12 h). At 20 h, explosive propagation occurred producing a large clump of condensed fibrils (Fig. 1*A*, 20 h). Because the background was still very dark, the propagation occurred predominantly near the hairpin-like fibril observed at 11 h.

In another case, a single linear fibril of about 15 μm was detected in darkness at 13 h. The growth of this fibril was monitored every 2 or 3 h (Fig. 1*B* and supplemental Movie S1). ThT fluorescence became intense in the middle of the fibril (Fig. 1*B*, 15 and 18 h). Then, a large number of fibrils emerged and elon-

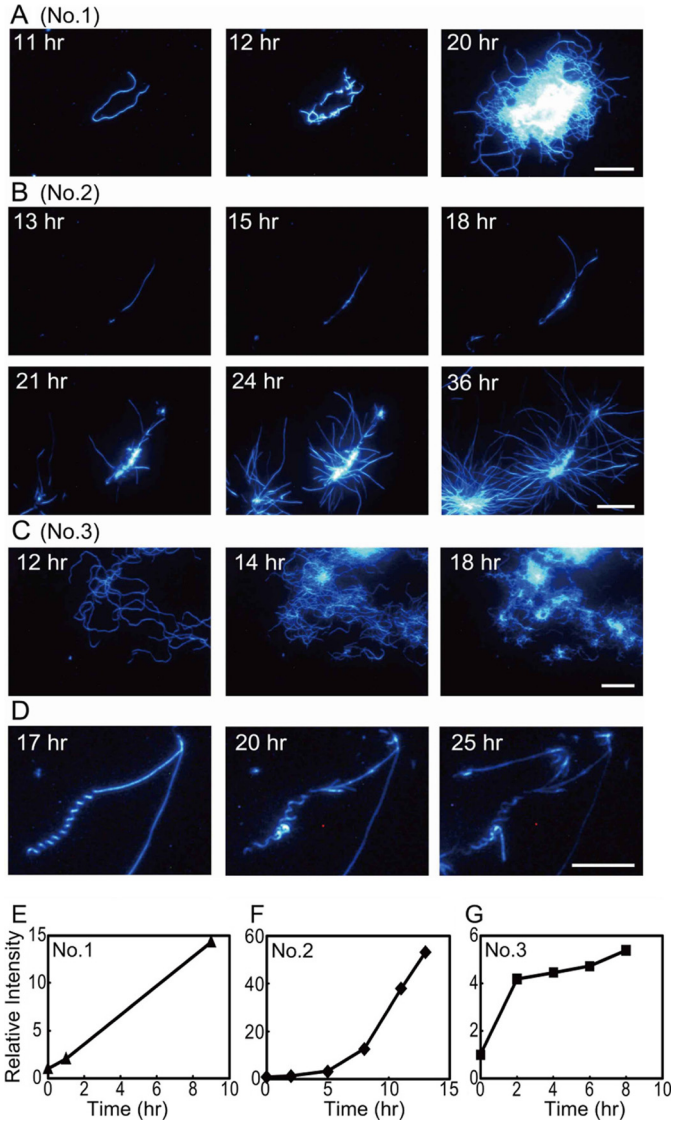

FIGURE 1. **Visualization of the laser-induced propagation of Aβ(1–40) fibrils.** *A* and *B*, real-time observations revealing explosive propagation from a single fibril. *C*, propagation of random walk-like fibrils with branching. *D*, mixed image of the laser-induced destruction and propagation of fibrils. The *scale bars* represent 10 μm. *E–G*, time courses of fibril propagation obtained by quantifying TIRFM images shown in *A–C*. *Abscissa* represents time after initiation of laser irradiation. The fibrils were monitored by laser irradiation of 3–5 s duration at the observation point. No. 1–3 indicate the numbering of quantified images, all of which are summarized in Fig. 5.

gated, forming a spherulitic structure with a core located in the original fibril (Fig. 1*B*, 21–36 h). In a previous study, we classified the supramolecular structure of Aβ(1–40) fibrils into three types (8): type 1, linear and rigid fibrils often formed by seed-dependent extension; type 2, spherulitic structures made of cooperatively elongating fibrils; and type 3, worm-like fibrils with a random walk morphology. The series of images in Fig. 1*B* illustrate one of the mechanisms responsible for the formation of spherulites. Secondary nucleation multiplies the number of seeds, thus producing a large number of fibrils concomitantly.

Among several morphological types, the worm-like type 3 fibril is of particular interest because it is composed of short and rigid fibril blocks, implying the presence of potential multiple active growing ends (8). We could also monitor the growth of worm-like fibrils in real-time (Fig. 1*C* and supplemental Movie S2). The random walk elongation forming long fibrils was detected at 12 h, the morphology consistent with our previous study (Fig. 1*C*, 12 h). After 2 h, new fibrils emerged from multiple points of preformed fibrils (Fig. 1*C*, 14 h). Finally, apparently entangled clusters of fibrils were formed. The newly formed fibrils seen at 18 h mostly were within the area where fibrils were observed at 12 h. These images suggest extensive branching or secondary nucleation within the worm-like fibrils observed at 12 h, consistent with an internal structure composed of short fibril blocks with potential active growing ends. Again, the background was very dark, supporting the notion that spontaneous nucleation is difficult in comparison with the propagation of preexisting fibrils.

These series of images emphasize that some kind of self-breakage occurred within the preformed fibrils, thus providing a scaffold for subsequent explosive propagation. The scaffold with many active growing ends in its vicinity combined with the type of fibril (*i.e.* straight or worm-like) defines the morphology of fibrils, leading to clumps of clustered fibrils in one case and spherulitic structures in another. Although the breaking up of fibrils as shown here evidently was accelerated by the laser beam, similar spherulitic structures have been reported to form in darkness without irradiation (8). In other words, when breakage or secondary nucleation occurs more easily than spontaneous nucleation, the fibril formation becomes a highly cooperative process accelerated by preexisting fibrils, leading to supramolecular structures with densely packed fibrils.

Additionally, we found a unique case involving the growth of a single fibril (Fig. 1*D*). A right-handed helical fibril was observed at 17 h. The helical structure had broken into several pieces at 20 h. At 25 h, some of the pieces had started to grow into new fibrils, whereas others continued to disappear.

To characterize the dependence of propagation on the type of fibrils (Fig. 1, *A–C*), we quantified the fibril images (No. 1–3) by plotting the total fluorescence intensity (*i.e.* amount of fibrils) against reaction time (Fig. 1, *E–G*, see also "Experimental Procedures"). It is noted that the data points show all the laser irradiation events applied to the fibrils and that abscissa represents the time after the first laser irradiation: 11 h in Fig. 1*A* was set to zero in Fig. 1*E*. Quantification of representative images (Fig. 1, No. 1–3) showed that the fluorescence intensity (*i.e.* amount of fibrils) increased variously with time (Fig. 1, *E–G*), suggesting the different types of growth, although the detailed characterization is difficult because of the limited amount of data, in particular for the case of Fig. 1*A*. In the case of Fig. 1*B*, the fluorescence intensity increased cooperatively with a lag phase (Fig. 1*F*). This cooperative growth has been often observed for the spontaneous fibril formation in bulk solution monitored by ThT assay, suggesting that the similar propagation also occurs in bulk solution (8). Interestingly, the growth curve of the worm-like type 3 fibrils was different from other two types (Fig. 1*G*). The fluorescence intensity increased in a saturating manner, suggesting that the worm-like fibrils have more active ends than other types. This is consistent with our previous observation that the worm-like fibrils retain a large number of potential growing ends (8).

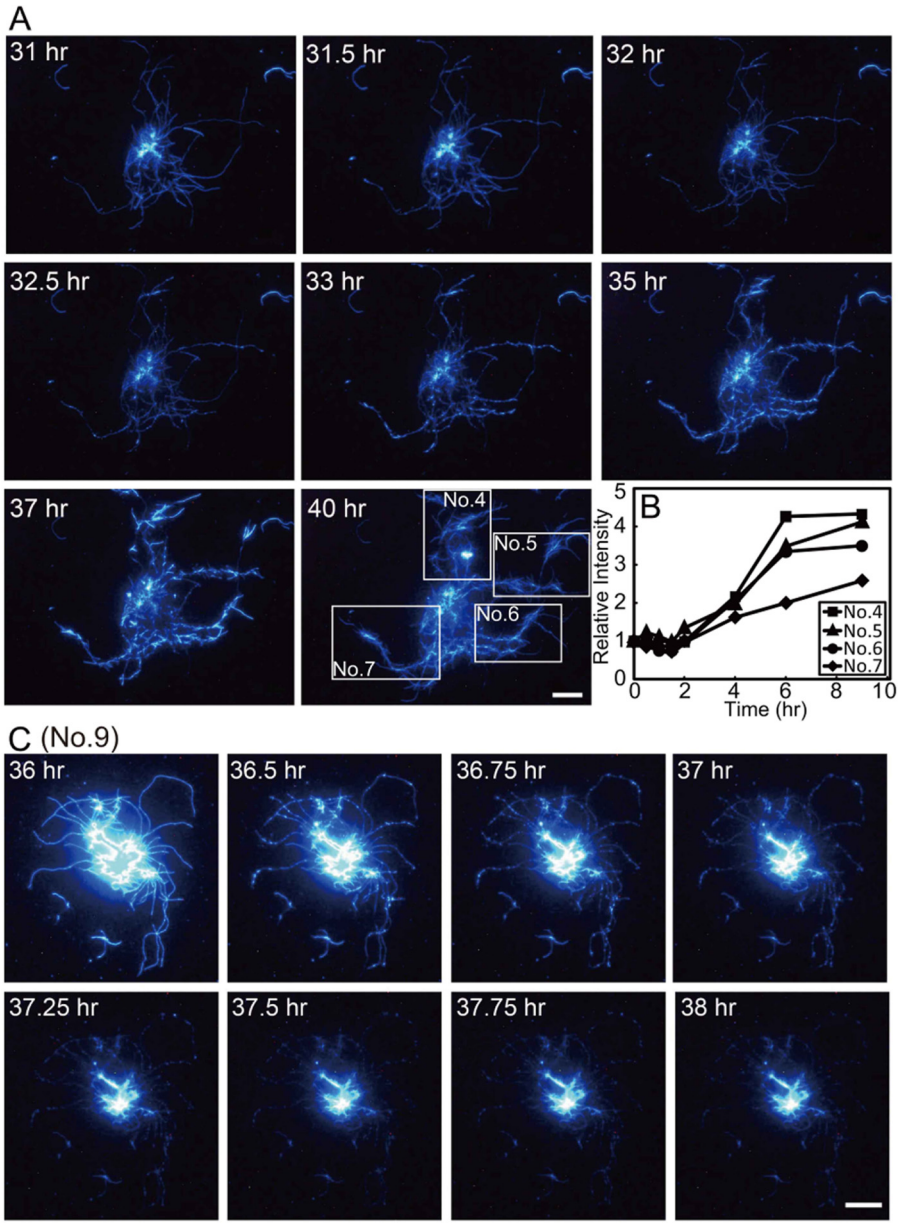

FIGURE 2. **Effects of an interval between laser irradiations on propagation and destruction of Aβ(1–40) fibrils.** *A*, propagation of new fibrils from preformed fibrils. *B*, time course of fibril propagation obtained by quantifying the regions No. 4–7 at 40 h of *A*. Detailed images were shown in supplemental Fig. S1. *C*, destruction of preformed fibrils by intermittent irradiation. The fibrils were monitored by laser irradiation of 3–5 s duration at the observation point. The *scale bars* represent 10 μm.

Effects of Laser Irradiation on Aβ(1–40) Fibril Growth—To examine whether the laser irradiation destructs or propagates the fibrils, preformed fibrils were irradiated at various time intervals (Fig. 2, supplemental Movies S3 and S4). When preformed fibrils were irradiated every 30 min, many brilliant fluorescence spots appeared on preexisting fibrils (Fig. 2*A*, 31–33 h). Then, when the laser irradiation was switched to every 2 or 3 h, a large number of new fibrils elongated from the fluorescence spots (Fig. 2*A*, 35–40 h). Still, the background was very dark, indicating that secondary nucleation occurred only on the preformed fibrils and the remaining monomers joined the fibril growth at the new active sites.

To confirm that the accelerated propagation is caused by the laser irradiation, we checked nonirradiated regions of the quartz plate (supplemental Fig. S1*E*). Even after 37 h, the straight fibrils without branching remained. The straight fibrils were distinct from the irradiation-induced fibrils, confirming that the laser beam critically accelerated fibril growth combined with partial destruction.

To characterize the laser-induced fibril propagation in detail, we quantified four areas (No. 4–7) from TIRFM images (Fig. 2*A*, 40 h, Fig. 2*B*; see also supplemental Fig. S1, *A–D*). Interestingly, all areas showed a growth curve similar to Fig. 1*B*. Again, the time is after the initiation of laser irradiation. These series of cooperative growth with a lag phase at a single fibril level are consistent with the growth curve in bulk solution, indicating that the secondary nucleation is essential for fibril propagation (8). A similar result was obtained for another set of experiment, confirming the reproducibility (supplemental Fig. S2).

We also examined the effects of laser irradiation for every 15 min, more frequent than before, on the clustered preformed fibrils (Fig. 2*C*). At first, brilliant fluorescence spots were observed on the preexisting fibrils, similar to Fig. 2*A* (Fig. 2*C*, 36–37 h). However, following intermittent irradiation every 15 min gradually decomposed the fibrils (Fig. 2*C*, 37.25–38 h). Although the cores of clustered fibrils resisted destruction, these results strongly suggest that propagation or destruction of fibrils depends on the laser dosage.

Destruction of Aβ(1–40) Fibrils by Irradiation—To focus on the inhibition or destruction of fibrils, we used the laser irradiation more frequently. In one case, a cluster of fibrils was detected after 14 h of incubation in darkness, and real-time observations were carried out every hour. The growth was inhibited by the laser (Fig. 3*A* and supplemental Movie S5). After 25 h, we interrupted the observation (*i.e.* stopped the irradiation) for several hours and then restarted them. During this period, new fibrils emerged, although some damaged fibrils did not change their morphology. The results suggest that the repeated irradiation critically damaged the fibrils leading to a loss of elongating ability (Fig. 3*A*, 33 h). In another case, growth continued for 21 h in darkness (*i.e.* without observation) on a quartz slide, producing a bundle of long and mature fibrils (Fig. 3*B*). Then, we started making observations every hour by applying laser irradiation.

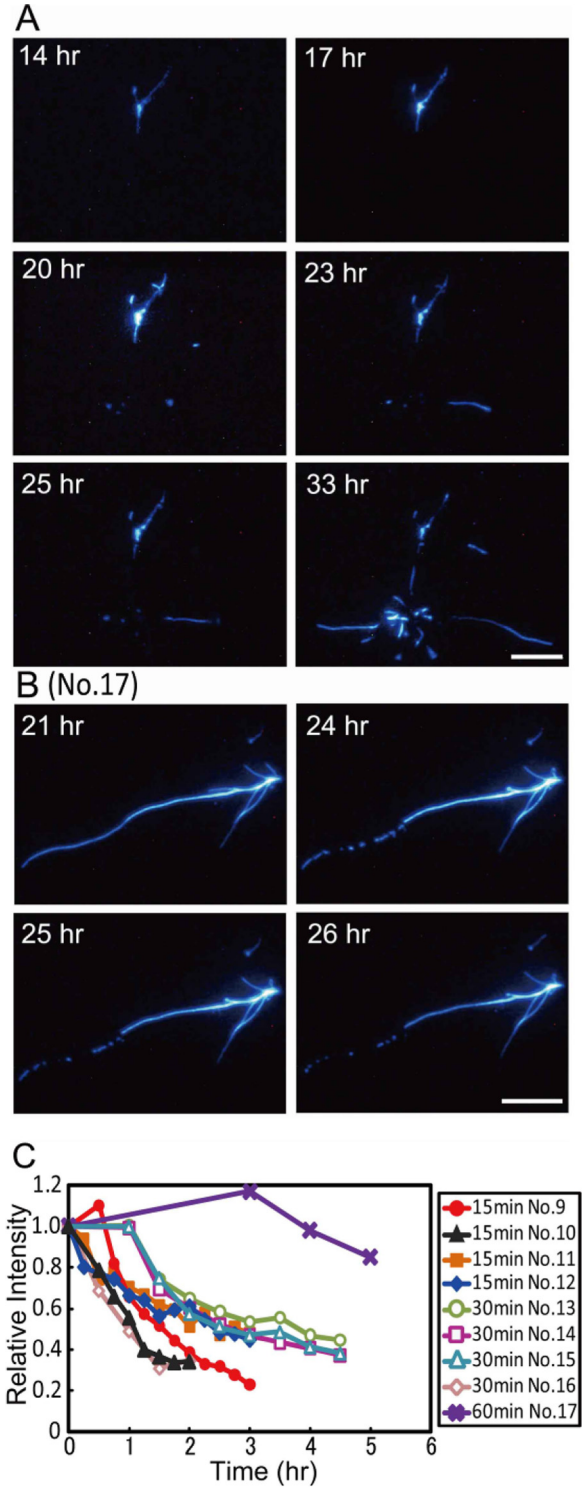

FIGURE 3. **Visualization of the laser-induced destruction of Aβ(1–40) fibrils.** *A*, effects of extensive laser irradiation on spontaneous Aβ(1–40) fibril growth. After 14 h, the fibrils were monitored every 1 or 2 h to 25 h, by laser irradiation of 3–5 s duration at the observation point. *B*, effect of extensive laser irradiation on preformed fibrils. Aβ(1–40) fibrils were prepared on quartz slides in the absence of irradiation. The elongated fibrils were then irradiated intermittently at an intensity of 40 milliwatts for 1 min. The *scale bars* represent 10 μm. *C*, dependence of fibril destruction on the interval of laser irradiation. The fibrils were monitored by laser irradiation of 40–55 milliwatts for 1 min at the observation point. Original data are shown in supplemental Figs. S3 and S4.

ThT fluorescence decreased in the thinner regions of the fibril (Fig. 3*B*, 24 h) and disappeared (Fig. 3*B*, 25 and 26 h), indicating a disruption of the fibrils by extensive irradiation.

To further investigate fibril disruption by laser irradiation, preformed fibrils were irradiated with various intervals between 15–60 min with a constant laser irradiation of 1-min duration (Fig. 3*C*, supplemental Figs. S3 and S4). TIRFM images were quantified, and the normalized data were plotted against a time. The decrease of intensity by laser irradiation every 60 min was slight. On the other hand, the intensity decreased significantly by intermittent irradiation of every 15 and 30 min. These results indicated that the destruction of fibrils depends on the dosage or total energy of laser irradiation.

We examined not only an interval of laser irradiation but also the dependence on the laser power (supplemental Fig. S5). The laser power was varied between 10 and 55 milliwatt with a 1-min duration every 30 min. The fibril destruction occurred only at 55 milliwatt laser power (supplemental Fig. S5*D*). Meanwhile, fluorescence intensity increased at 10 milliwatt laser power, indicating that low laser power propagated fibrils. These various images taken together indicate that the growth under irradiation is a dynamic process determined by a balance between the destruction of preformed fibrils and partial destruction-triggered acceleration of fibril growth.

Effects of Irradiation in Bulk Solution—To analyze the effects of irradiation on the polymerization and chemical structure of Aβ(1–40), we performed experiments in a bulk solution (Fig. 4 and supplemental Fig. S6). The fibrils were prepared in a glass cell with a 10-mm light path and then set on the TIRFM stage. Because even a very low concentration of SDS prevents an analysis of mass, the experiments were performed with fibrils prepared in the absence and presence of 0.5 mM SDS, and the mass was checked only for the sample without SDS. Similar results were obtained for the fibrils prepared in the presence of 0.5 mM SDS.

The cell was irradiated with a laser beam at 442 nm at a power of 30–40 milliwatt for 24–40 h under continuous agitation with a stirrer tip. During the continuous irradiation, the intensity of ThT fluorescence decreased and the light scattering intensity decreased slightly (Fig. 4*A* and supplemental Fig. S6*A*). In contrast, without irradiation, the intensities of ThT fluorescence and light scattering remained constant, although both increased slightly at 5 h and then returned to original values at 20 h (Fig. 4*A* and supplemental Fig. S6*A*). To examine the participation of ThT, an experiment was carried out in the absence of ThT. The light scattering intensity did not change (supplemental Fig. S6*B*), confirming that a combination of laser irradiation and ThT is essential for the destruction of Aβ(1–40) fibrils.

To compare the size distribution of fibrils with and without laser irradiation, we performed analytical ultracentrifugation (Fig. 4, *B* and *C*, and supplemental Fig. S6, *C* and *D*). As expected from the large size of amyloid fibrils, Aβ(1–40) fibrils without irradiation precipitated rapidly at 664 × *g* (Fig. 4*B* and supplemental Fig. S6*C*). Under the same conditions, the fibrils after irradiation precipitated slowly and ~20% (corresponding to absorbance of 0.08–0.1) remained unprecipitated (Fig. 4*C*

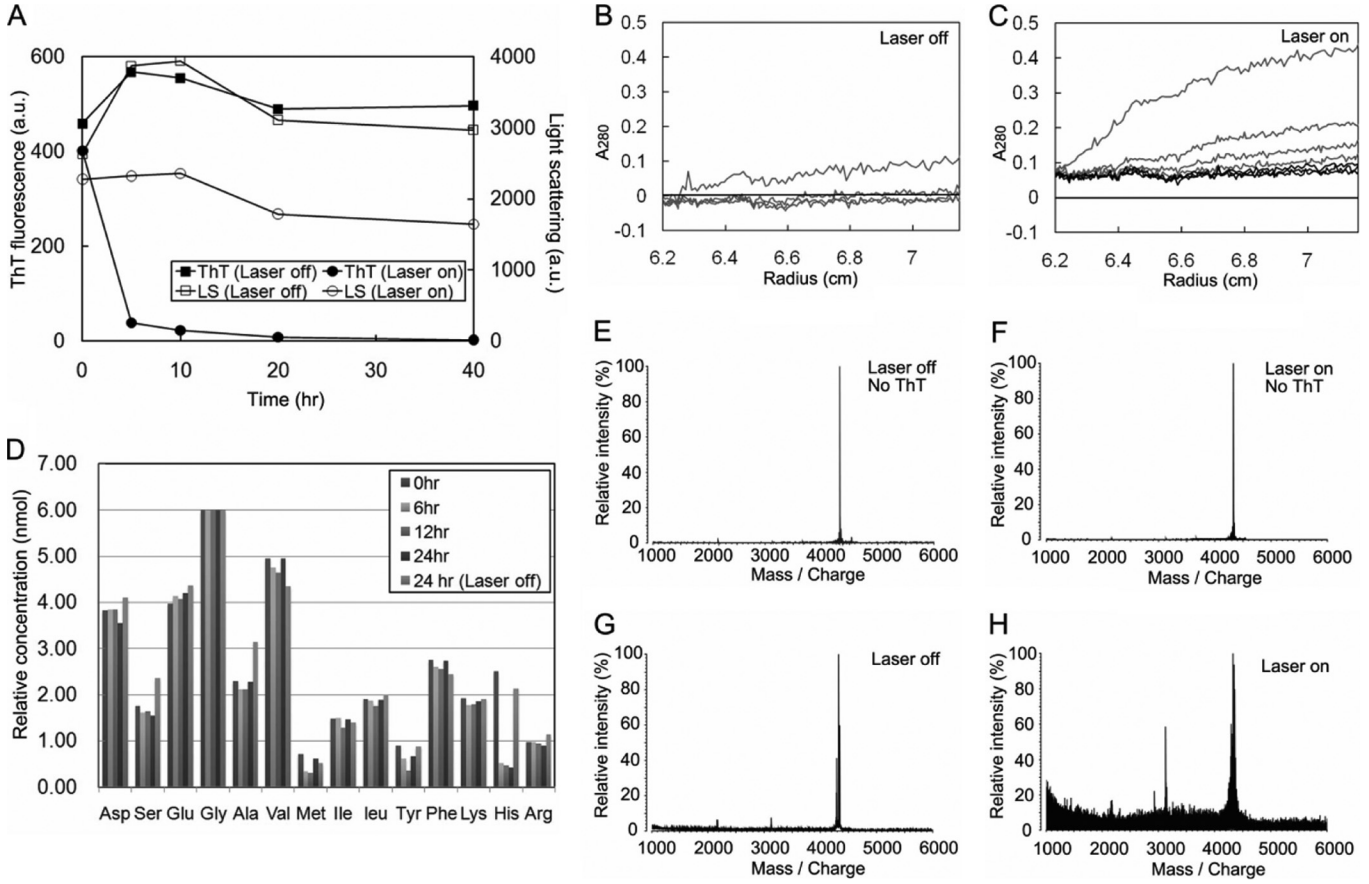

FIGURE 4. **Analyses of the laser-irradiated Aβ(1–40) fibrils in a glass cell.** The irradiation was performed at 442 nm. *A*, kinetics of the disruption of fibrils monitored using ThT fluorescence (●, ■) and light scattering (○, □) with (●, ○), or without (■, □) laser irradiation. *B* and *C*, the sedimentation pattern of fibrils without (*B*) or with (*C*) laser irradiation. Sedimentation patterns were recorded at 3,000 rpm (664 × *g*) (*B* and *C*, *gray lines*) and 53,000 rpm (207,270 × *g*) (*C*, *black lines*) by monitoring the absorbance at 280 nm, and several traces at intervals of 2 min (3,000 rpm) or 30 min (53,000 rpm) are presented. *D*, identification of chemical modifications by amino acid analysis. *E–H*, mass spectra. *E*, the reference spectrum of Aβ(1–40) fibrils without irradiation or ThT, after laser irradiation without ThT (*F*), without irradiation in the presence of ThT (*G*), and after irradiation in the presence of ThT (*H*).

and supplemental Fig. S6*D*). When we raised the rotor speed to 207,270 × *g*, at which Aβ(1–40) monomers precipitate in several hours, the remaining fraction started to precipitate (Fig. 4*C* and supplemental Fig. S6*D*). The results suggested that the laser partly depolymerized amyloid fibrils with ~20% of the molecules depolymerized completely into monomers and shorter fragments.

Our previous study has shown that active oxygen is involved in the laser-dependent destruction of K3 fibrils (19). To address the chemical modifications, we performed an amino acid analysis (Fig. 4*D* and supplemental Fig. S6*E*). The Aβ(1–40) peptide is composed of three Asp, one Asn, two Ser, three Glu, one Gln, six Gly, three Ala, six Val, one Met, two Ile, two Leu, one Tyr, three Phe, two Lys, three His, and one Arg residue. Among the five types of amino acids susceptible to oxidation (*i.e.* Met, Cys, Tyr, Trp, and His), Aβ(1–40) contains one Met, one Tyr, and three His residues. After 6 h of irradiation, the His content decreased to <0.5, indicating chemical modification by the laser. In contrast, for the reference sample without irradiation, it remained above 2.0 even after 24 h. The Met content decreased to below 0.5 even at time zero, probably because the agitation of samples accelerated oxidation. Although the amount of Tyr was not quantified, similar oxidation reactions may also occur for the Tyr residue. Therefore, although we did not analyze quantitatively Met and Tyr residues, it is likely that they were also modified by the excitation of amyloid-bound ThT.

Finally, a mass analysis was performed for the fibrils prepared in the absence of SDS (Fig. 4, *E–H*). When we examined the effects of the laser on Aβ(1–40) fibrils in the absence of ThT, we could not detect any chemical modification or fragmentation (Fig. 4*F*) compared with the reference sample without irradiation (Fig. 4*E*). Thus, the irradiation by itself did not decompose Aβ(1–40) fibrils. In the presence of ThT, the Aβ(1–40) fibrils without irradiation were similar to those of the reference sample (Fig. 4, *E–G*). On the other hand, the Aβ(1–40) fibrils irradiated in the presence of ThT revealed several peaks representing decomposed peptides (*m*/*z*, 1450.1; 2166.0; 2173.8; 2876.8; 2934.7; and 3134.6) as well as the peak for the Aβ(1–40) monomer (*m*/*z*, 4330.8), indicating the chemical destruction caused by the irradiation (Fig. 4*H*).

On the basis of the *m*/*z* values, we predicted the corresponding amino acid sequences: ^{6}HDSGYEVHHQKL^{17} for *m*/*z* 1450.1 (1449.5); ^{1}DAEFRHDSGYEVHHQKLVFFAEDV^{24} for *m*/*z* 2876.8 (2876.1); ^{1}DAEFRHDSGYEVHHQKLVFFAEDVG^{25} for *m*/*z* 2934.7 (2933.1); and ^{3}EFRHDSGYEVHHQKLVFFAEDVGSNKG^{29} for *m*/*z* 3134.6 (3133.1), where the values in parentheses indicate the calculated average mass (supplemental Fig. S7). These calculations suggest His and Tyr

residues located at the N-terminal region to be the targets of active oxygen. The structure of amyloid fibrils of Aβ(1–40) has been proposed based on solid state NMR spectroscopy (25, 26). Although the details depend on experimental conditions, the C-terminal region is buried by the lateral association of protofibrils. On the other hand, the N-terminal (1–8, unstructured; 9–21, β-strand; and 22–29, loop) is likely to be exposed to solvent. It is intriguing that the peptides recovered are mostly from the N-terminal region.

DISCUSSION

Laser-induced Inhibition and Destruction of Aβ(1–40) Fibrils—The laser-induced inhibition and destruction are likely to be the same as those for K3 fibrils (19), and the mechanism is similar to that used for photodynamic therapy, in which active oxygen plays a critical role. Photodynamic therapy involves the use of photochemical reactions of light with photosensitizing agents, inducing the generation of various types of active oxygen (27, 28). The substrate can further react with oxygen molecules to produce superoxide anions, which can then create hydroxyl radicals. The radicals have been shown to carry out reactions of backbone fragmentation with model peptides (29). In the case of amyloid fibrils, the amyloid-bound ThT exhibits strong fluorescence at ~485 nm when excited at 442 nm by a He-Cd laser. The excited ThT may transfer energy to ground state molecular oxygen, producing singlet oxygen and moreover oxygen peroxide and oxygen radicals. Additionally, excited triplet oxygen generates hydrogen peroxide and various types of free radicals. These radicals attack nearby amyloid fibrils causing various chemical modifications, ultimately leading to the depolymerization and decomposition of Aβ(1–40) fibrils. The results contrast with reports that, in some neurodegenerative disorders, active oxygen generated from amyloid fibrils induces apoptosis (22, 30).

Laser-induced Propagation of Fibrils—Remarkably, we also observed an accelerating effect of the laser on propagation after the apparent inhibition or destruction of growing fibrils. Although this was unexpected, the mechanism is straightforward. The breaking up of preformed fibrils increases the number of active ends, thus leading to an acceleration of fibril growth. If this partial destruction occurs more frequently than forming a new nucleus, explosive propagation around the preformed fibrils will occur, producing crowded and possibly entangled clusters of fibrils or spherulitic structures.

It is evident that explosive propagation, as observed here, is accelerated by the laser-assisted destruction of amyloid fibrils. However, we noticed that the spontaneous formation of Aβ(1–40) fibrils conducted in darkness often produced a similar supramolecular morphology, *i.e.* spherulites, and entangled amyloid clusters or clumps (8). Thus, it is likely that breakage and secondary nucleation play important roles, particularly in spontaneous fibril formation even in the absence of laser-assisted destruction. In other words, when spontaneous nucleation is slow or unlikely to occur, the role of secondary nucleation including breakage or branching becomes more important than in the case of seed-dependent fibril growth, where the overall growth rate is high and depends largely on the number of original seeds. The various brilliant images of Aβ(1–40) amyloid clusters against the dark background obtained for spontaneous fibril formation support this view (8).

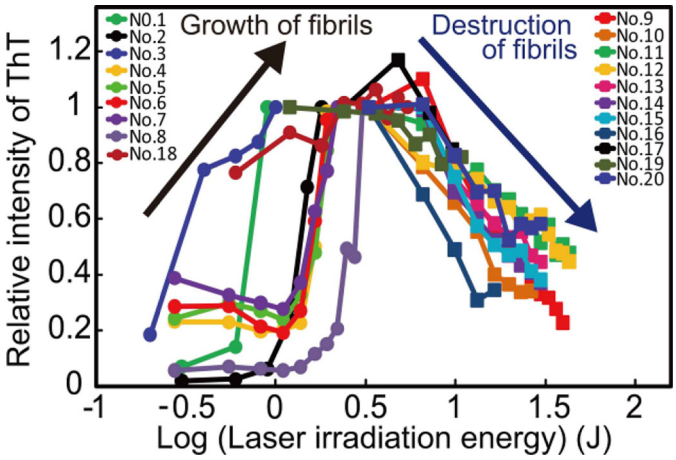

FIGURE 5. **Laser irradiation-dependent propagation and destruction of Aβ(1–40) fibrils leading to a profile with an optimum.** All the quantified kinetic data of laser-dependent propagation (No. 1–8) or destruction (No. 9–17) of fibrils are plotted. The plot also includes the data of the dependence on the laser power (No. 18–20). Quantified ThT intensities were normalized to be one for the end points of fibril propagation and for the starting points of fibril destruction. *Abscissa* in log scale represents a total irradiation energy calculated by multiplying the laser power by the total irradiation period in seconds.

Recently, Andersen *et al.* (14) reported a branching mechanism for fibrils of glucagon. Moreover, secondary nucleation has been suggested to be important for other amyloidogenic proteins and peptides (*e.g.* insulin, huntingtin, and islet amyloid polypeptide) (31–33). Thus, although various mechanisms of secondary nucleation have been proposed (breakage, fork, diffusion, and branching), the process is thought to be essential for propagation of fibrils. Our results visualize one example of secondary nucleations at the single fibril level, propagating dramatically the amyloid fibrils.

Propagation Profile with an Optimum against Structural Perturbation—The growth of fibrils under irradiation is a dynamic process determined by a balance between the destruction of preformed fibrils and partial destruction-triggered acceleration of fibril growth. To clarify the combined effects, we plotted all the quantified kinetic data of laser-dependent propagation (Fig. 5, No. 1–8) or destruction (Fig. 5, No. 9–17) of fibrils. The plot also includes the data of the dependence on the laser power (Fig. 5, No. 18–20). Because the amount of fibrils represented by the fluorescence intensity varied significantly depending on the experiment and the image area quantified, we normalized the intensities to be one for the end points of propagation kinetics and for the starting points of destruction kinetics. As abscissa, we used a total irradiation energy calculated by multiplying the laser power (watts = J/sec) by the total irradiation period in seconds. Although the exact energy applied to each of the fibrils is unknown, this normalization permits the comparison of various data under different conditions with the same TIRFM equipment. To scatter the data of laser-induced propagation, *abscissa* is in log scale.

Importantly, the plot showed an optimum in the amount of fibrils (Fig. 5). Although we have to obtain more quantitative and statistical data, the profile with an optimum suggests that

the rate of propagation (or amount of fibrils) is determined by a balance between partial damage increasing the number of active ends and complete destruction inactivating any seeding potential (supplemental Fig. S8). Until a critical point is reached, the propagation rate increases with an increase in laser energy. Beyond this critical point, the irradiation works adversely, inactivating the seeding potential of fibrils. To create effective therapeutic strategies, it is important to verify both the laser energy-dependent propagation and destruction of amyloid fibrils. Furthermore, considering that template-dependent self-propagation is the most essential property of fibril formation, this kind of profile with an optimum may be common to various variables that destabilize amyloid fibrils. For example, high concentrations of denaturants (*e.g.* urea and guanidine hydrochloride) can unfold fibrils (34). However, at low concentrations of denaturants, partial denaturation is expected to propagate the fibrils. Moreover, several compounds are suggested to decompose amyloid fibrils (35). Compounds that simply destabilize amyloid fibrils are anticipated to increase the number of active ends and thus have adverse effects. From a therapeutic viewpoint, rather than destabilizing or breaking down fibrils, inhibitors that inactivate seeding potentials by capping the active ends may be preferable.

Conclusion—In conclusion, we succeeded in visualizing the fragmentation-dependent propagation of individual amyloid fibrils in real-time. Moreover, we revealed that the fate, propagation, or destruction of Aβ(1–40) fibrils depends on the energy or dosage of the laser irradiation (Fig. 5 and supplemental Fig. S8). In other words, the formation or degradation of fibrils can be achieved by manipulating the power of the laser and duration. Although the underlying mechanism by which ThT binds to amyloid fibrils remains unclear (36–38), the advantage of ThT is that it binds specifically to the fibrils, allowing one to concentrate regions of photodynamic therapy. Thus, if effective compounds similar to ThT were to become available, photodynamic therapy very specific to amyloid fibrils may become possible, suggesting that the use of a laser to destroy amyloid fibrils does have potential.

Acknowledgments—We thank Drs. Tetsuichi Wazawa (Tohoku University) and Tadato Ban (Fukui University) for support with the TIRFM system. We also thank Miyo Sakai for help with the analytical ultracentrifugation.

REFERENCES

1. Dobson, C. M. (2003) *Nature* **426,** 884–890
2. Cohen, F. E., and Kelly, J. W. (2003) *Nature* **426,** 905–909
3. Chiti, F., and Dobson, C. M. (2006) *Annu. Rev. Biochem.* **75,** 333–366
4. Fowler, D. M., Koulov, A. V., Balch, W. E., and Kelly, J. W. (2007) *Trends Biochem. Sci.* **32,** 217–224
5. Maji, S. K., Perrin, M. H., Sawaya, M. R., Jessberger, S., Vadodaria, K., Rissman, R. A., Singru, P. S., Nilsson, K. P., Simon, R., Schubert, D., Eisenberg, D., Rivier, J., Sawchenko, P., Vale, W., and Riek, R. (2009) *Science* **325,** 328–332
6. Ban, T., Yamaguchi, K., and Goto, Y. (2006) *Acc. Chem. Res.* **39,** 663–670
7. Krebs, M. R., Macphee, C. E., Miller, A. F., Dunlop, I. E., Dobson, C. M., and Donald, A. M. (2004) *Proc. Natl. Acad. Sci. U.S.A.* **101,** 14420–14424
8. Yagi, H., Ban, T., Morigaki, K., Naiki, H., and Goto, Y. (2007) *Biochemistry* **46,** 15009–15017
9. Ban, T., Morigaki, K., Yagi, H., Kawasaki, T., Kobayashi, A., Yuba, S., Naiki, H., and Goto, Y. (2006) *J. Biol. Chem.* **281,** 33677–33683
10. Librizzi, F., and Rischel, C. (2005) *Protein Sci.* **14,** 3129–3134
11. Padrick, S. B., and Miranker, A. D. (2002) *Biochemistry* **41,** 4694–4703
12. Mauro, M., Craparo, E. F., Podestà, A., Bulone, D., Carrotta, R., Martorana, V., Tiana, G., and San Biagio, P. L. (2007) *J. Mol. Biol.* **366,** 258–274
13. Tanaka, M., Collins, S. R., Toyama, B. H., and Weissman, J. S. (2006) *Nature* **442,** 585–589
14. Andersen, C. B., Yagi, H., Manno, M., Martorana, V., Ban, T., Christiansen, G., Otzen, D. E., Goto, Y., and Rischel, C. (2009) *Biophys. J.* **96,** 1529–1536
15. Higurashi, T., Hines, J. K., Sahi, C., Aron, R., and Craig, E. A. (2008) *Proc. Natl. Acad. Sci. U.S.A.* **105,** 16596–16601
16. Tipton, K. A., Verges, K. J., and Weissman, J. S. (2008) *Mol. Cell* **32,** 584–591
17. Ban, T., Hoshino, M., Takahashi, S., Hamada, D., Hasegawa, K., Naiki, H., and Goto, Y. (2004) *J. Mol. Biol.* **344,** 757–767
18. Ban, T., Hamada, D., Hasegawa, K., Naiki, H., and Goto, Y. (2003) *J. Biol. Chem.* **278,** 16462–16465
19. Ozawa, D., Yagi, H., Ban, T., Kameda, A., Kawakami, T., Naiki, H., and Goto, Y. (2009) *J. Biol. Chem.* **284,** 1009–1017
20. Krishnan, S., Chi, E. Y., Wood, S. J., Kendrick, B. S., Li, C., Garzon-Rodriguez, W., Wypych, J., Randolph, T. W., Narhi, L. O., Biere, A. L., Citron, M., and Carpenter, J. F. (2003) *Biochemistry* **42,** 829–837
21. Olteanu, A., and Pielak, G. J. (2004) *Protein Sci.* **13,** 2852–2856
22. Bieschke, J., Zhang, Q., Bosco, D. A., Lerner, R. A., Powers, E. T., Wentworth, P., Jr., and Kelly, J. W. (2006) *Acc. Chem. Res.* **39,** 611–619
23. Wazawa, T., and Ueda, M. (2005) *Adv. Biochem. Eng. Biotechnol.* **95,** 77–106
24. Naiki, H., Higuchi, K., Hosokawa, M., and Takeda, T. (1989) *Anal. Biochem.* **177,** 244–249
25. Petkova, A. T., Yau, W. M., and Tycko, R. (2006) *Biochemistry* **45,** 498–512
26. Paravastu, A. K., Leapman, R. D., Yau, W. M., and Tycko, R. (2008) *Proc. Natl. Acad. Sci. U.S.A.* **105,** 18349–18354
27. Giuliano, E. A., Ota, J., and Tucker, S. A. (2007) *Vet. Ophthalmol.* **10,** 337–343
28. Buytaert, E., Dewaele, M., and Agostinis, P. (2007) *Biochim. Biophys. Acta* **1776,** 86–107
29. Davies, M. J. (2003) *Biochem. Biophys. Res. Commun.* **305,** 761–770
30. Allsop, D., Mayes, J., Moore, S., Masad, A., and Tabner, B. J. (2008) *Biochem. Soc. Trans.* **36,** 1293–1298
31. Smith, J. F., Knowles, T. P., Dobson, C. M., Macphee, C. E., and Welland, M. E. (2006) *Proc. Natl. Acad. Sci. U.S.A.* **103,** 15806–15811
32. Dahlgren, P. R., Karymov, M. A., Bankston, J., Holden, T., Thumfort, P., Ingram, V. M., and Lyubchenko, Y. L. (2005) *Nanomedicine* **1,** 52–57
33. Ruschak, A. M., and Miranker, A. D. (2007) *Proc. Natl. Acad. Sci. U.S.A.* **104,** 12341–12346
34. Narimoto, T., Sakurai, K., Okamoto, A., Chatani, E., Hoshino, M., Hasegawa, K., Naiki, H., and Goto, Y. (2004) *FEBS Lett.* **576,** 313–319
35. Ono, K., Hamaguchi, T., Naiki, H., and Yamada, M. (2006) *Biochim. Biophys. Acta* **1762,** 575–586
36. Stsiapura, V. I., Maskevich, A. A., Kuzmitsky, V. A., Turoverov, K. K., and Kuznetsova, I. M. (2007) *J. Phys. Chem. A* **111,** 4829–4835
37. Groenning, M., Olsen, L., van de Weert, M., Flink, J. M., Frokjaer, S., and Jorgensen, F. S. (2007) *J. Struct. Biol.* **158,** 358–369
38. Biancalana, M., Makabe, K., Koide, A., and Koide, S. (2009) *J. Mol. Biol.* **385,** 1052–1063

Laser-induced Propagation and Destruction of Amyloid β Fibrils

Hisashi Yagi, Daisaku Ozawa, Kazumasa Sakurai, Toru Kawakami, Hiroki Kuyama, Osamu Nishimura, Toshinori Shimanouchi, Ryoichi Kuboi, Hironobu Naiki and Yuji Goto

J. Biol. Chem. 2010, 285:19660-19667.
doi: 10.1074/jbc.M109.076505 originally published online April 20, 2010

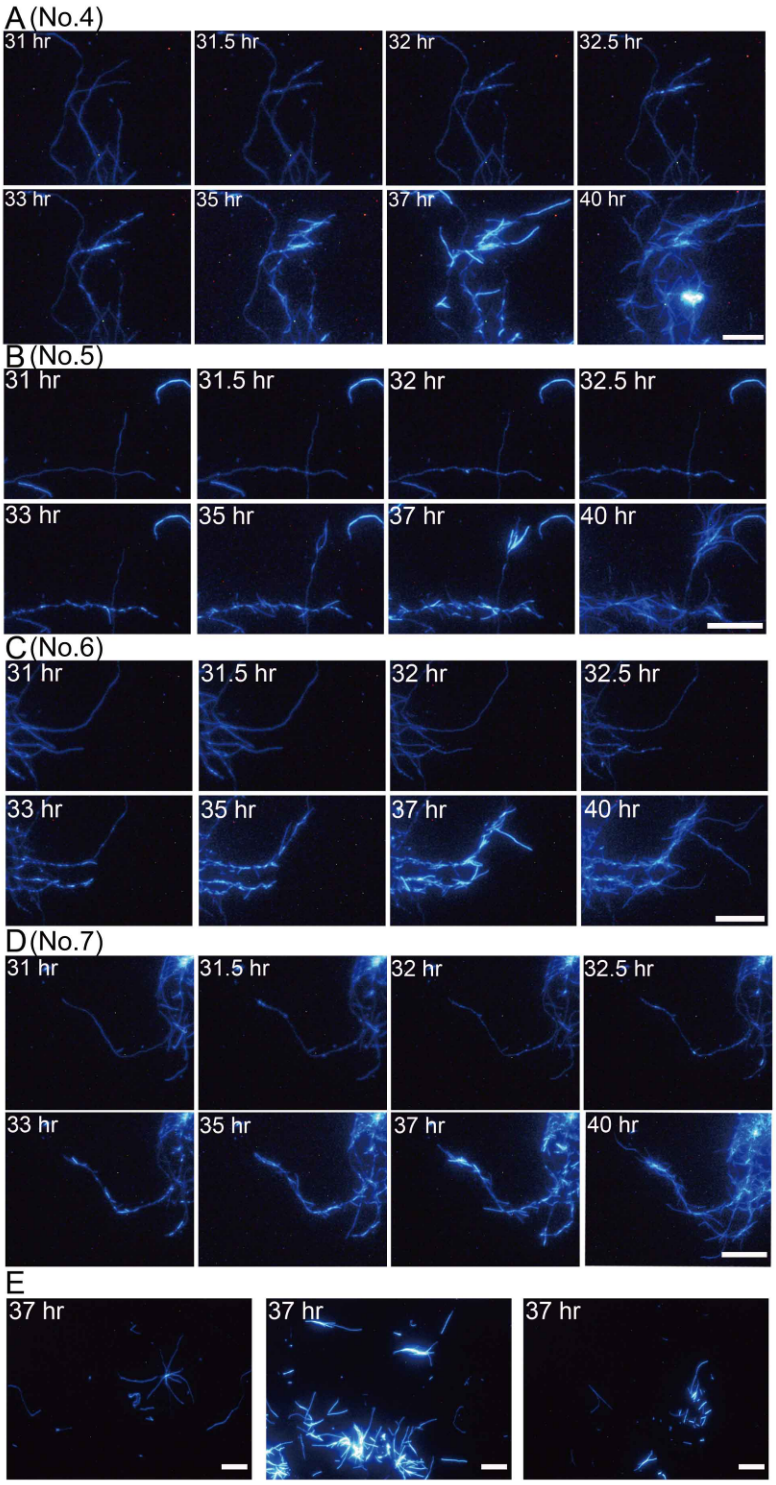

SUPPLEMENTAL Fig. S1

Analysis of laser-induced propagation of Aβ(1-40) fibrils by TIRFM. *A-D*, Fig. 2A was divided into 4 areas as indicated in Fig. 2A for quantitative analyses. *E*, The images of non-irradiated areas after 37 hr. The scale bars represent 10 μm.

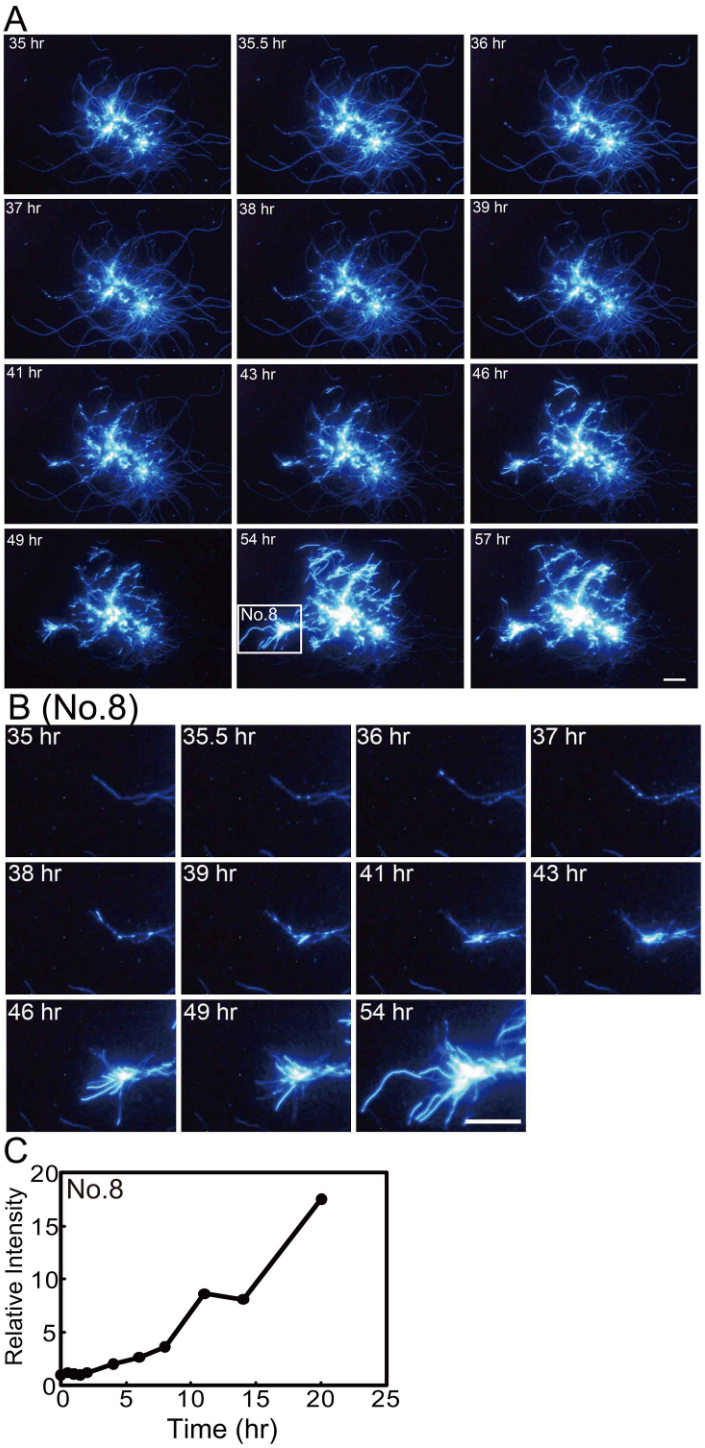

SUPPLEMENTAL Fig. S2

Visualization of the laser-induced propagation of Aβ(1-40) fibrils from preformed fibrils. *A,* Whole images of real-time observation of fibril propagation from preformed fibrils. *B*, Extended images of fibril propagation taken from *A*. *C*, Time course of fibril propagation obtained by quantifying TIRFM images shown in *B*. The scale bars represent 10 μm.

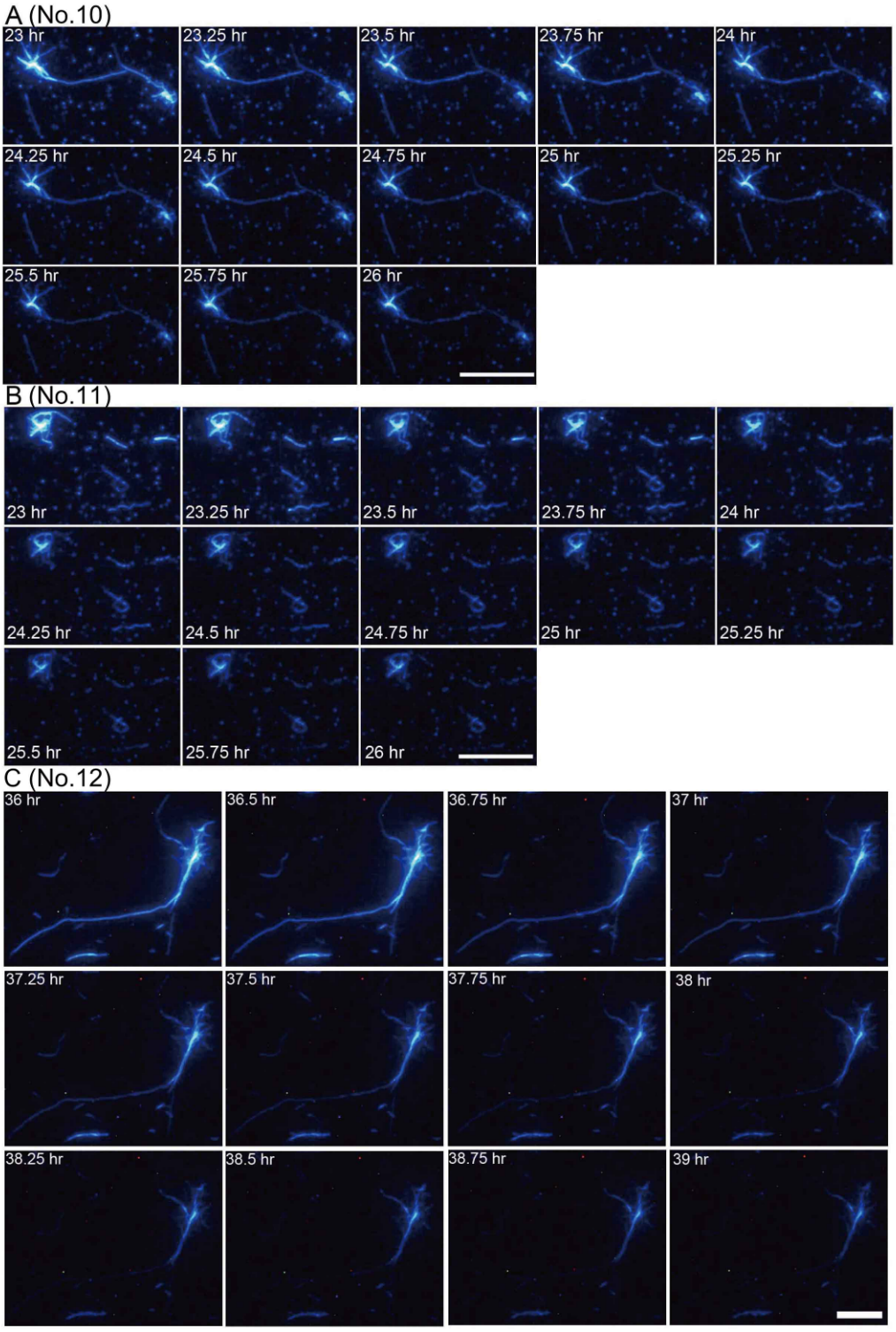

SUPPLEMENTAL Fig. S3

Destruction of Aβ(1-40) fibrils by extensive laser irradiation every 15 min. *A-C*, Effects of extensive laser irradiation on preformed fibrils. The elongated fibrils were then irradiated intermittently at an intensity of 55 mW for 1 min at the observation point. The scale bars represent 10 μm.

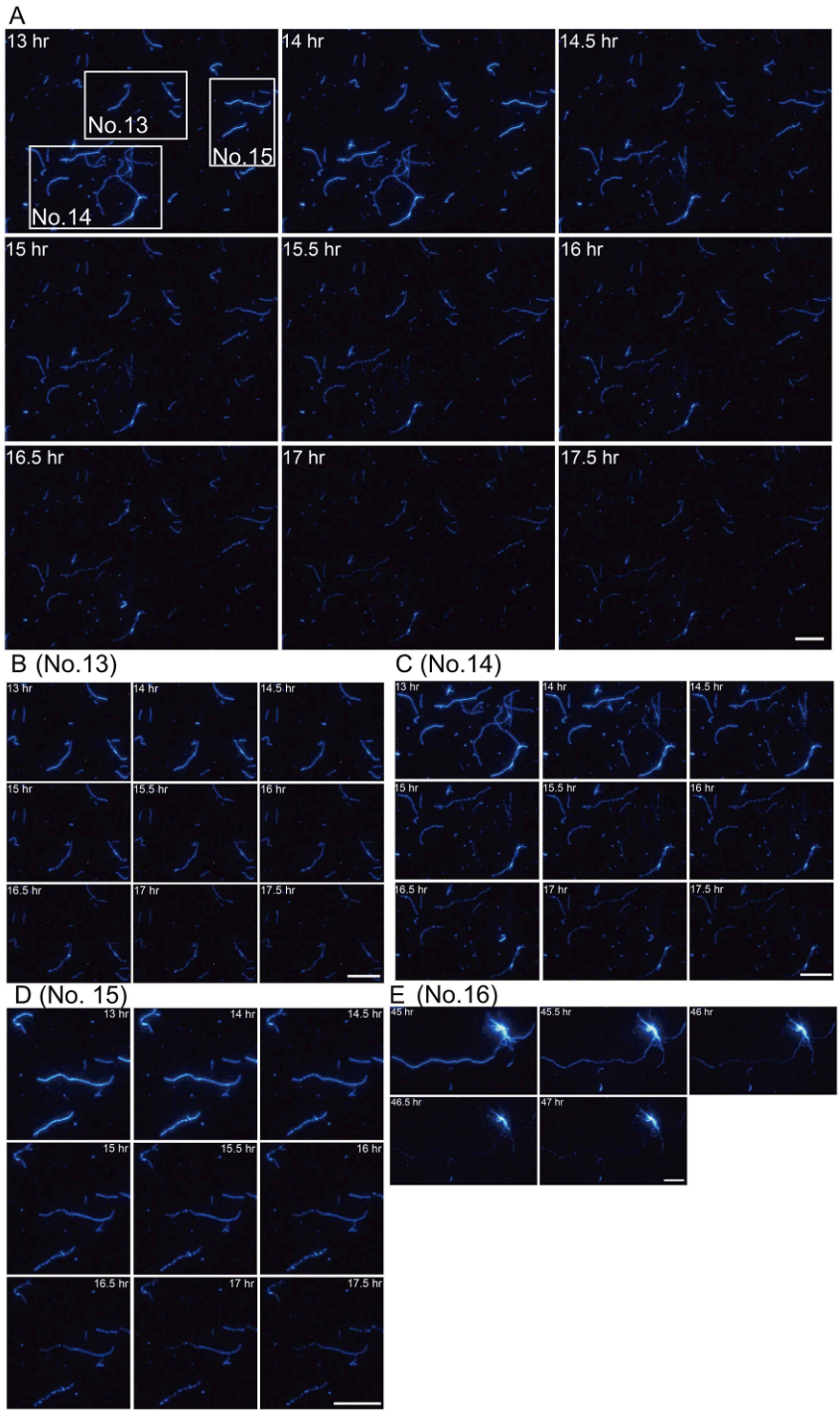

SUPPLEMENTAL Fig. S4

Destruction of Aβ(1-40) fibrils by extensive laser irradiation every 30 min. *A,* Whole images of real-time observation of fibril destruction from preformed fibrils. *B-D*, Extended images of fibril propagation taken from *A* for quantitative analysis. *E*, Fibril destruction obtained from the separate experiment. The elongated fibrils were then irradiated intermittently at an intensity of 55 mW for 1 min at the observation point. The scale bars represent 10 μm.

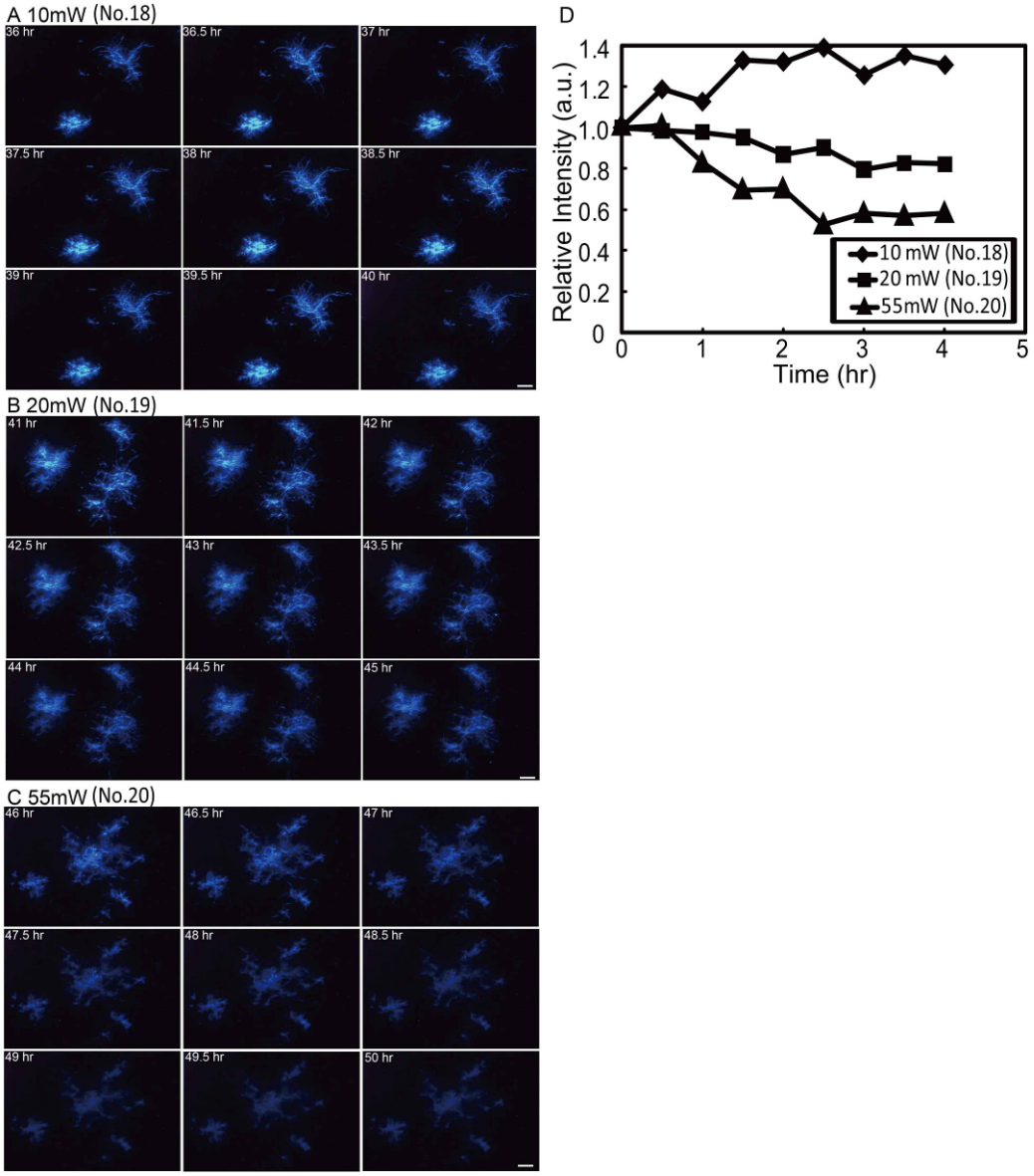

SUPPLEMENTAL Fig. S5

Dependence of Aβ(1-40) fibril destruction on the laser power. *A-C,* The laser power was varied between 10 and 55 mW (*A*: 10 mW, *B*: 20 mW, *C*: 55 mW). The elongated fibrils were irradiated for 1 min at the observation point. *D*, Time course of fibril propagation or destruction obtained by quantifying TIRFM images shown in *A-C*. The scale bars represent 10 μm.

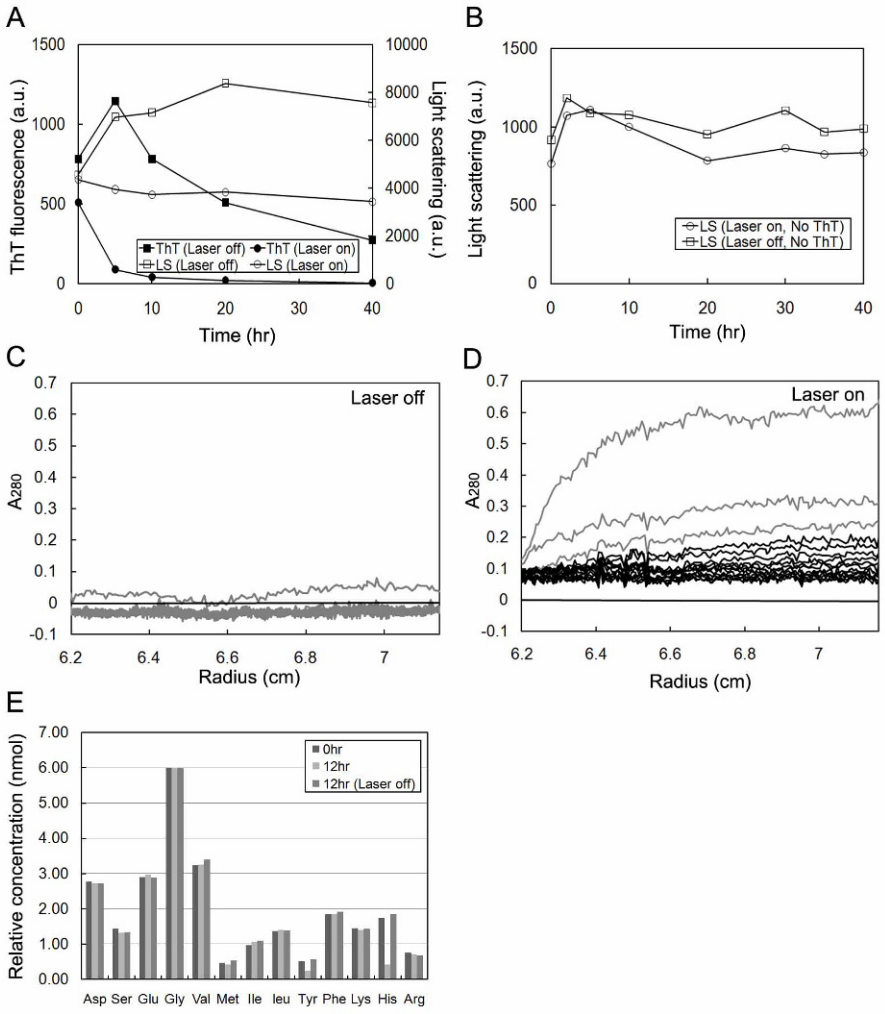

SUPPLEMENTAL Fig. S6

Analyses of the laser-irradiated Aβ(1-40) fibrils in a glass cell in the presence of 0.5M NaCl and 0.5 mM SDS. *A*, Kinetics of the disruption of fibrils were monitored using ThT fluorescence (●, ■) and light scattering (○, □) with (●, ○) or without (■, □) laser irradiation. *B*, Effects of laser irradiation in the absence of ThT (○: laser on, □: laser off) monitored by light scattering. *C* and *D*, The sedimentation pattern without (*C*) or with (*D*) laser irradiation. Sedimentation patterns were recorded at 3,000 rpm (664 x g) (*C* and *D*, gray lines) and 45,000-53,000 rpm (149,420-226,000 x g) (*D*, black lines) by monitoring the absorbance at 280nm, and several traces at intervals of 2 min (3,000 rpm), 8 min (45,000rpm) or 30 min (53,000 rpm) are presented. *E*, Identification of chemical modifications of Aβ(1-40) by amino acid analysis. The irradiation was performed at 442 nm under the same conditions as shown in a. Apparently, His residues were oxidized by the laser. Moreover, it was thought that Met and Tyr residues were oxidized.

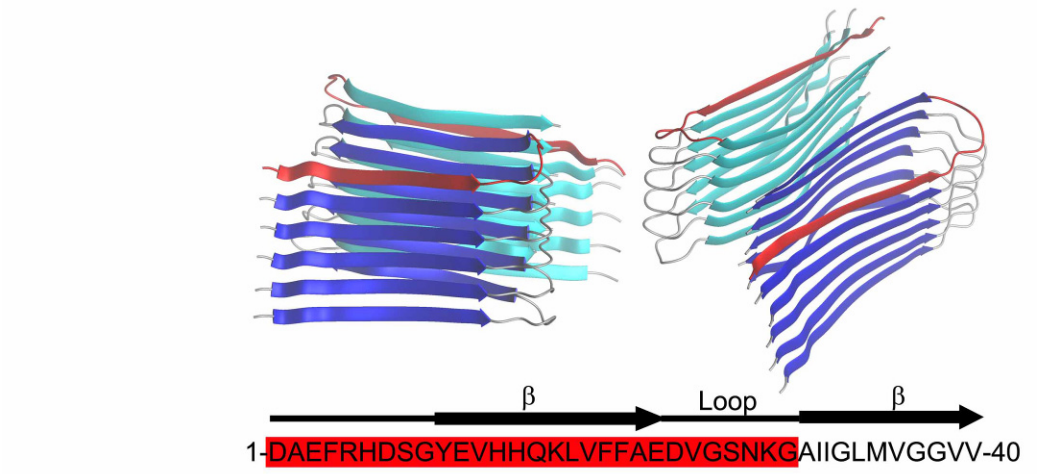

1. 1450.1 (1449.5): 6-HDSGYEVHHQKL-17
2. 2876.8 (2876.1): 1-DAEFRHDSGYEVHHQKLVFFAEDV-24
3. 2934.7 (2933.1): 1-DAEFRHDSGYEVHHQKLVFFAEDVG-25
4. 3134.6 (3133.3): 3-EFRHDSGYEVHHQKLVFFAEDVGSNKG-29

SUPPLEMENTAL Fig. S7

The amino acid sequences of Aβ(1-40) peptides recovered after laser irradiation at 442 nm. The structures of Aβ(1-40) fibrils have been proposed by Petokova et al. (Petkova et al. *Biochemistry*, 45, 498-512 (2006)). Numbers indicate obtained mass values, while those in parentheses indicate the theoretical values. Red indicates the 1-29 region of Aβ(1-40) accommodating most of the recovered peptides.

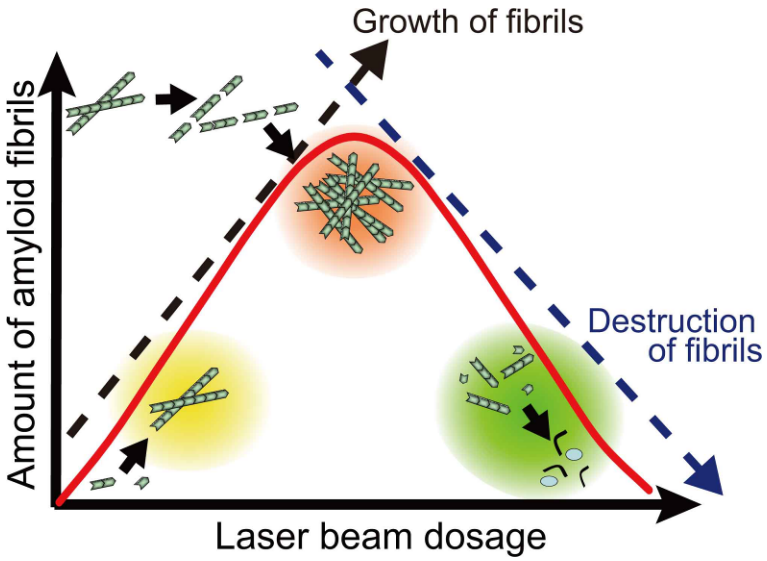

SUPPLEMENTAL Fig. S8
Schematic illustration of the relationship between the amount of fibrils and laser beam dosage. The amount of amyloid fibrils is determined by a balance between the laser-induced propagation and laser-induced destruction of fibrils. First, the irradiation partially destroys fibrils and thus increases the number of seeds, leading to an acceleration of fibril growth. However, extensive irradiation inactivates the self-propagating potential of fibrils and ultimately destroys the fibrils completely.

SUPPLEMENTAL MOVIES

Supplemental Movie S1
Real-time observation of Aβ(1-40) fibril propagation. The spontaneous fibril formation was monitored every 2 or 3 hr. At 15hr, a single linear fibril was detected. Upon further incubation, new fibrils elongated from the single linear fibril (18-36 hr).

Supplemental Movie S2
Real-time observation of worm-like Aβ(1-40) fibril propagation. The growth of worm-like fibrils was monitored every 2 hr. The new fibrils elongated from multiple points of preformed fibrils (16-20hr).

Supplemental Movie S3
Laser-induced propagation of preformed Aβ(1-40) fibrils. The growth of fibrils was monitored every 2 or 3hr. First, preformed fibrils were irradiated by laser every 30 min (31-33 hr). Then, the interval of laser irradiation was switched to 2 or 3 hr, leading to new fibril elongation (35-40 hr).

Supplemental Movie S4
Laser-induced destruction of preformed Aβ(1-40) fibrils. First, brilliant fluorescence spots were observed on the preformed fibrils (36-37 hr). Continuing intermittent laser irradiation every 15 min disrupted the fibrils (37.25-38 hr).

Supplemental Movie S5
Real-time observation of the laser-induced inhibition of Aβ(1-40) fibril growth. The growth of fibrils was inhibited by intermittent irradiation every hour. After 25hr, the observation was interrupted for several hours and then restated. Although the new fibrils emerged, some damaged fibrils did not change their morphology.